Chemical analysis of silica doped hydroxyapatite biomaterials consolidated by a spark plasma sintering method

J.L. Xu†, K.A. Khor

School of Mechanical & Aerospace Engineering, Nanyang Technological University, 50 Nanyang Avenue, Singapore 639798

Abstract

Silica (SiO_2) and the silicate-based biomaterials play an important role due to their *in vitro* and *in vivo* biological response. The present study synthesized a novel nano-structured amorphous silica doped hydroxyapatite (HA) via an aqueous precipitation route. HA was prepared with 0, 1, 3 and 5 wt% silica, which are comparable to the measured silicon content of natural bone. After spray drying into micron sized powders, the silica doped HA (SiHA) powders were consolidated at 1000 ℃ with a dwell time of 3 min using a spark plasma sintering (SPS) technique. X-ray diffraction analysis showed a main apatite phase with minor secondary β-tricalcium phosphate (β-TCP) was observed in the as-consolidated SiHA compacts. Substitution of PO_4^{3-} by SiO_4^{4-} in the apatite structure resulting in a small increase in the lattice parameters in both a-axis and c-axis of the unit cell were identified by X-ray photoelectron spectrometer (XPS) analysis and Raman spectrometer investigation. The cell culture *in vitro* investigation demonstrated that the presence of silicon in the SPS consolidated compacts contributed to the relatively high cell proliferation ability when compared with phase pure HA.

Keywords: Silica; Hydroxyapatite; Spark plasma sintering; Substitution

† Corresponding author Tel: 65 6790 4349 fax: 65 6792 4062 E-mail: jlxu@ntu.edu.sg

1. Introduction

Hydroxyapatite ($Ca_{10}(PO_4)_6(OH)_2$, HA) has been introduced as a bone grafting materials due to its chemical composition similar to those of natural bone. However, its medical application has been limited because the low mechanical properties, relatively long time for remodeling and slow rate of osseointegration [1]. Therefore it is essential to improve the mechanical properties and bioactivity for the long-term application.

Synthesis of chemically modified or ion-substituted HA [2] has drawn great interest since the ions played an important role in developing artificial bone with enhanced mechanical properties and bioactivities. Except for the appropriate mechanical properties, biocompatibility was the most important feature of an implant. It is reported that the silicate ions into HA structure improved its *in vivo* bioactivity [3] and Si-substituted HA became an attractive alternative to conventional HA materials for use as bone substitute compacts. Silicate ion substitution was also reported to enhance the formation of a poorly crystalline surface apatite layer of HA after immersing in simulated body fluids (SBF) [4]. Current ideas concerning the role of silicon in biological functions were related to the ability of silicon in the form of silicic acid ($Si(OH)_4$) [5].

Many approaches have been used to prepared silicon substituted HA (Si-HA) [2,6,7]. A popular method was postulated by Gibson et al. [7] by developing an aqueous precipitation technique to prepare silicon-substituted HA. A co-substituted HA has been prepared using high temperature solid-state methods which required the substitution of a second ion such as lanthanum in addition to silicon [8].

A rapid consolidation process based on spark plasma activation has been widely studied as energy source to consolidate samples to high densities from the powder form [9,10]. Compared with conventional consolidation methods which need long processing time at high temperature, the novel spark plasma sintering (SPS) enables fast sintering within several minutes at relatively low temperature by Joule heat and spark plasma generated by high-pulsed electric current through the compact. The most important character of SPS is that the powder is heated by spark discharge between

the particles. As a result, the sample would be sintered uniformly and rapidly from both inside and outside. During SPS process, a strong electrical field is produced in the small gaps of the particles to make the electrons, cations and anions strike the surface of the opposite particle and activate the particles. Thus some chemical reactions would occur during this process.

The aim of the present study was to prepare a new nano-structured hydroxyapatite-based material by a spark plasma sintering process and study the biological behavior of the consolidated materials. A small level of precipitated silica (SiO_2, 0, 1, 3 and 5 wt%) was introduced in an HA slurry which was subsequently spray-dried into powder form. The spray dried powders were consolidated using SPS method. The surface chemistry that would directly influence the cell proliferation was characterized through advanced analysis methods. The mechanical properties of the bulk compacts were evaluated with a micron hardness tester. An *in vitro* test is carried to investigate the cell proliferation responses of osteoblast (bone forming cell) on various silica doped biomaterial surfaces.

2. Experimental details

An HA slurry was prepared using a wet chemical approach by reacting 0.6 mol of orthophosphoric acid (H_3PO_4) with 1 mol of calcium hydroxide ($Ca(OH)_2$). The precipitation reactants were carried out at 40 ± 5 ℃ in house and terminated when the pH was reached 9 through the addition of H_3PO_4. After the complete mixing of the reactants, the precipitate was stirred for two more hours and left overnight to settle. Amorphous precipitated silica as preset weight was added into the HA slurry and the slurry was stirred for four more hours before transportation into a spray dryer (Ohkawara LT-8, Japan), where the atomization and drying processes took place.

A spark plasma sintering system (Sumitomo Coal Mining SPS system, Dr. Sinter Modal 1050, Japan) was used to consolidate the various powder feedstock to get the following ceramic samples: ceramic HA (from phase pure spray dried HA), ceramic 1SiHA (from the powder doped with 1 wt% of silica), ceramic 3SiHA (from the powder doped with 3 wt% of silica) and ceramic 5SiHA (from the powder doped with

5 wt% of silica). During the SPS system operation, one gram of loose powder feedstock was loaded in a graphite die (13 mm in diameter) and punch unit. A relatively low pressure of 7.5 MPa was initially applied. The sintering temperature was 1000 °C with a dwell time of 3 min at a heating/cooling rate of 100 °C/min. The consolidated ceramic samples were ground till Grit P 2400 for the following characterization.

A field emission scanning electron microscope (FE SEM, JEOL 6340F) was used for the powder surface morphology analysis. An SEM (JEOL 5600LV, Japan) was employed for the fracture surface analysis for the consolidated samples. Phases and lattice parameters were identified using X-ray diffraction (XRD) (Philips MPD 1880, the Netherland) using Cu K_α radiation at 30 kV and 20 mA. The XRD analysis was carried through the 2θ from 20 ° to 60 ° at a scan rate of 0.04˚ per second. Raman spectra of the samples were recorded at room temperature and atmospheric pressure on Renishaw Raman Imaging Microscope (United Kingdom). The excitation source was formed by a 632 nm line of a HeNe laser that attached to the microscope to provide a confocal illumination of the sample via a holographic beam splitter. The chemical composition of the SPS compacts was determined by X-ray photoelectron spectroscopy (XPS). XPS spectra were recorded on a Kratos spectrometer (Japan) operated using Al Kα (1486.6 eV) monochromatic X-ray source. The XPS pressure was about 10^{-9} Pa. Since apatites are insulators, the spectra were shifted towards higher binding energies due to the accumulation of positive charge on the surface. In the case of apatite, the calibration was done by referencing to P 2p (133.6 eV) because the binding energy of this element did not change very much in apatite [11] due to the screening of the P atom by oxygen atoms, and to a close crystalline potential.

The mechanical properties of these SPS compacts were studied in hardness (*H*) and Young's modulus (E) using a micro-hardness tester (CSEM® MHT, Switzerland) as micro-indentation subjected very small materials volumes to mechanical forces. The maximum load was 1N with a dwell time of 10 s at a loading/unloading rate of 2 N/min. During the test for E determination, every two points had a distance of 200 μm to avoid the stress-strain influence caused by previous loading the preceding

indentation. The average values were calculated from ten readings for each compacted sample.

After the samples (ceramic HA, ceramic 1SiHA and 5SiHA) were sterilized via autoclaving, confluent human limb-derived osteoblasts were passaged by trypsin-EDTA and then seeded with an initial cell density of 2×10^4 /cm^2 onto the samples that were placed in a 24-well culture tray and incubated at 37 °C in a 5% CO_2 atmosphere. The culture medium used for each sample was 1 ml of Dulbecco's modified Eagle's medium/F12 supplemented with 10 vol% of fetal bone bovine serum and 5 vol% of antibiotics. The medium was replaced with an equal volume of fresh medium every 2 days. A methyl thiazole tetrazodium (MTT) assay was employed to examine the proliferation of the cells for 2 and 4 days. The plates were read using 490 nm wavelength on a micro-plate reader machine (Benchmark Plus, Bio-Rad Laboratories Inc.). The cell attachment was observed under SEM (JEOL JSM-5600 LV, Japan) after cell culture for 24 h. The cells on the bioceramic surfaces were fixed in 2.5% glutaraldehyde buffered in 0.1 M sodium cacodylate (pH 7.3-7.4) for 1 h at 4 ℃ following by 30 min treatment in 1% tannic acid in 0.1 M sodium cacodylate at 4 ℃. The post fixation was processed with 1% OsO4 buffered in 0.1 M sodium cacodylate for 30 min at 4 ℃. Following post fixation, the samples were rinsed with distilled water for 10 min, and dehydrated in a graded series of ethanol for 5-10 min at room temperature. Finally the samples were immersed in increasing concentrations of hexamethyldisilazane (HMDS), which was a mixture of HMDS and ethanol, for critical point drying. After removing the HMDS solution and drying the sample in the dryer, they were gold sputtered for 120 s at 10 mA to allow observation under the SEM.

3. Results and discussion

3.1 Powders characterization

The SEM micrograph of the received spray-dried HA powders without doping silica (Figure 1a) showed that the HA powder contained nano-sized particles. Under higher magnification as shown in Figure 1b, these nano-sized particles had actually

needle shape with a length of ~100 nm and a width of ~30 nm. The amorphous silica was made up of nano-sized granules as shown in Figure 1c. After spray-drying process, the silica homogeneously distributed in the spray-dried SiHA powders (Figure 1d).

Figure 2a presented the XRD patterns of spray dried powders doped with various amount of amorphous silica. A single-phase apatite was observed in all these four kinds of apatite powders; and no secondary phase, such as tricalcium phosphate (TCP, $Ca_3(PO_4)_2$) was detected by the XRD analysis. The broadening of the peaks indicated that the spray dried (SD) powders were mainly made up of relatively fine particles as observed in Figure 1.

3.2. Phase stability, silicon substitution and surface chemistry of SPS compacts

Fig. 3 showed the XRD patterns of the SPS consolidated HA with and without doping amorphous silica. No any other peak than HA was traced in the ceramic HA as observed. While, when silica-doped HA was densified at the same working conditions, it was found that the apatite structure became less stable and a secondary phase of β-TCP was detected in all the compacts doped with silica. This finding indicated that the presence of silica enhanced the decomposition process of HA. Referred to the relative intensities of β-TCP, it was found that its content increased with an increase in the amount of doping silica. Ruys [12] reported similar detection that the introduction of silica would lead to the decomposition of HA into secondary calcium phosphate phases such as TCP. They also suggested the decomposition of HA was reduced from the usual range of ~1300 to 1400 ℃ down to ~750 to 1150 ℃ in the presence of the additives such as Al_2O_3, SiO_2 and C. The reduction in decomposition temperature varied according to the composition of additives. In this study, the amorphous precipitated silica resulted in the HA becoming less stable at the sintering temperature of 1000 ℃. In addition, the impact of spark plasma might cause a localized increase in temperature and introduce some liquid phase of silica which did not form a strong chemical bond with apatite, and the presence of liquid phase would reduce interfacial energy and promote the transformation of apatite phase to β-TCP phase that would

lead to the poor biodegradation characteristics of HA compacts and induce the natural bone ingrowth for extended periods.

Table 1 lists the lattice parameters (a and c) of the SPS compacts which were determined through the *(hkl)* peaks positions of apatites from XRD patterns according to the following formula [13]:

$1/d^2 = 4/3 \cdot (h^2+hk+k^2) / a^2 + l^2/c^2$

d was the lattice distance obtained from XRD results. Compared to the lattice parameters of phase pure ceramic HA, those of SiHA compacts were relatively large. Concerning the silicate and phosphate groups, the average lengths of the Si-O and P-O bonds were 1.62 Å [8] and 1.51Å [8], respectively. The substitution of PO_4^{3-} by SiO_4^{4-} was assumed to contribute to the increase in the lattice parameters of these SiHA compacts.

Typical phosphate vibrations modes of apatite were shown in Raman spectra as presented in Fig. 4. The positions of the peaks observed are listed in Table 2. The strongest line situated at around 962 cm^{-1} was attributed to the symmetric stretching ν_1 mode of PO_4^{3-}. The peaks situated at about 1040-1090 cm^{-1}, 571-603 cm^{-1} and 430-450 cm^{-1} were assigned, respectively, to the antisymmetric stretching ν_3, the antisymmetric bending ν_4 modes and the bending ν_2 of the PO_4^{3-} ions [14-16]. Since the similar vibrational structure of silicate and phosphate, no special peaks assigned to silicate were able to be directly differentiated from the present Raman spectra. It was found that the intensities of hydroxyl absorption band at 3571 cm^{-1} were slightly lower than that of phase pure ceramic HA. It indicated that the presence of silica might accelerate the breakdown process of the hydroxyl group in HA, and some vacancies or oxygen ion may substitute the hydroxyl sites and lead to a distortion of the hexagonal symmetry. The distortion of the hexagonal symmetry would lead the decomposition of apatite into β-TCP as shown in Figure 3. The formation of OH vacancies has been proven to be able to accelerate cation transport in the HA lattice and thus accelerate the whole sintering process [17] as well as decomposition process.

As proposed by Sayer et al [18], there should be full charge compensation for the loss of OH^-. Two possibilities were assumed to compensate the charged defects

formed by the loss of OH^-. The first was the oxygen-deficient or O^{2-} vacancies that would lead to the formation of pores. The second was the presence of excess calcium Ca^{2+} and these positively charged defects would be charge-compensated by the substitution of SiO_4^{4-} substitution in PO_4^{3-} in the consolidated specimen. A chemical analysis technique, XPS, has been used to investigate the possible replacement of PO_4^{3-} by SiO_4^{4-} in silicon-contained apatite by Balas et al. [19]. In the current study, XPS was also applied to detect the replace possibility of silicate substitution. XPS wide scan of the elements present in consolidated samples was shown in Figure 5. Ca 2p, Ca 2s, P 2s, P 2p, O 1s, C 1s and Si 2p were identified for all test conditions.

Typical narrow scan XPS spectra of ceramic 3SiHA were presented in Fig. 6. The P 2p peak was symmetric, which indicated its binding energy was quite stable in apatite. It was referenced at 133.6 eV. The Ca 2p spectrum showed a doublet with Ca $2p_{3/2}$ at 347.5 eV and Ca $2p_{1/3}$ at 351.1 eV. The O 1s peak showed an asymmetry and was fitted using the peak deconvolution approach. It was decomposed into three components. The main component at 532.1 eV corresponded to the O linked only to a phosphorous atom as in PO_4^{3-} ions. The second at higher energy (534.0 eV) was attributed to Si-O peak. The lowest peak at 535.2 eV corresponded to C-O peak. The C 1s was deconvoluted to three peaks which corresponded to aliphatic carbon atoms (284.5 eV), α-carbon atoms (285.6 eV) and carbonate (288.8 eV). The detection of carbon should be due to the absorbance of CO_2 and the graphite die also contributed to the presence of carbon. The Si 2p spectrum has decomposed into 103.5 and 102.3 eV, with an area intensity ratio of about 2:1. As reported by Mekki et al. [20], the binding energy of SiO_4^{4-} in sodium silicate was centered at 102.0±0.2 eV. According to peak of SiO_2 was centered at 103.9 eV [21], the first component in the current specimen was assigned to $Si\text{-}O_2$ and thus the higher oxidation peak was attributed to silicon atoms belonging to isolated SiO_4^{4-}. Table 3 listed the binding energies obtained from the various compacts. The variations in binding energies reflected the differences in the electronic environment of the Si element, the relatively low value of the binding energies of silicon in 5SiHA sample may be due to the depolymerization

degree of the SiO_4 units [19]. The silicate depolymerization might lead to increased numbers of Ca-O-Si units and fewer Si-O-Si units, which might result in the formation of calcium silicate. Thus it was assumed that HA decomposed into TCP and CaO that could react with silica to form calcium silicate. However, no calcium silicate could be observed from the XRD patterns, which was due to either too small amount or silicate substituted into apatite structure.

The role of the silicon substitution that entered the crystal structure should be clearly separated from those of sintering additives or aids [22] that were typically discrete second phases in the compacts. Normally, the sintering additives or aids were typically compounds with low melting points that promoted liquid-phase sintering to enhance the densification. Silica as sintering aids [21] in the traditional sintering of HA might form liquid phase by the melting of this sintering aid. The present XRD results, Raman analysis and XPS results indicated that silicon was being partially substituted into HA but no secondary phase such as calcium silicate which might behave as a sintering aid was observed.

As discussed by Gibson [1], if silicate substituted for phosphate (B type) with the concomitant loss of a hydroxyl group, vacancies would be introduced on the hydroxyl site as the level of silicon substitution was increased, but no cation vacancies were introduced. Under this case, the hydroxyl groups in the SiHA interacted more strongly with the calcium or silicate groups compared with HA and thus high sintering temperature was needed to improve the mobility of hydroxyl group for fully sintered compacts. In contrast, however, where silicate substituted for only hydroxyl groups, A type, the A type substitution did not generate the same number of vacancies as B type or AB type and limit the mobility of OH groups that were instrumental in the densification.

3.3. Densities and mechanical properties of SPS compacts

The average densities and relative densities of sintered specimen were listed in Table 4. The theoretical density of stoichiometric HA was 3.156 g/cm^3. It was found after sintering at 1000 ℃ for 3 min, the obtained densities of sintered samples

decreased with the increase of doping levels of silica. Although the relatively density of amorphous silica (2.2 g/cm^3) may contribute to the sintered density, the small amounts should not be considered in this study. The formation of pores (as shown in Fig. 7) and the phase transformation of HA into β-TCP mainly contributed to the decreased densities. The SEM micrographs of the fracture surfaces presented in Fig. 7 indicated that the fracture modes were fully transgranular. Few pores were detected on the phase pure ceramic HA compact while some intergranular porosity occurred in the SiHA compacts. The presence of porosities were formed due to the release of hydroxyl group from HA structure [23] and β-TCP would exist near the pores. As shown in Fig. 7, the grain sizes (less than 1 μm) of SiHA compacts were obviously finer than that of phase pure ceramic HA compacts (around 5 μm), showing that silica could suppress the densification and effectively impede the grains coarse during SPS processing.

Fig. 8 showed the dependence of Vickers hardness (H) and Young's modulus (E) on the amount of doping silica. The relatively low hardness obtained for the doped samples was mainly attributed to the low bulk density of the material. It was believed that the higher density has played a role in producing higher hardness values where an increase in density could lead to an increase in hardness [24-25].

The E value of sintered SD HA without silica was around 89 GPa. With an increase in the amount of doping silica from 1 to 5 wt %, the E values increased about 15% from 84GPa to 100GPa. As the densities of SiHA compacts were all slightly less than that of phase pure ceramic HA at the sintering temperature of 1000 ℃, the relatively higher E of these SiHA compacts might be mainly attributed to the relatively finer grains caused by the presence of silica impeding the grain growth.

3.4. In vitro test

The typical osteoblast morphologies on ceramic 5SiHA under SEM were exhibited in Figure 9 after fixation. It was found that the cells had attached on the sample surface after 2 days of cell culture. The majority of the cells had a flattened appearance with a predominantly polygonal morphology. A rough texture was

observed due to the presence of numerous blebs on the surface of the cells. The cells were attached to the biomaterials exhibiting filopodia-like with various lengths and lamelliapodia-like extensions. Close contact between the cells and the substrate was established through extending filopodia, which initiated the cellular anchorage on the substrate. This result indicated that the SPS sample surfaces provided preferential sites for cell attachment an in return, would recruit proteins and other growth factors to enhance the cellular activity.

The data from MTT assay reflected the ability of cell proliferation and cytotoxicity on the ceramic surfaces. The higher the MTT results, the more the viable cells. As shown in Fig. 10, the culture of osteoblast cells on the biomaterials showed no big differences in proliferation after culture for 2 days on ceramic HA and ceramic 5SiHA, though relatively higher results were observed on ceramic 1SiHA. After 4 days of cell culture, comparison between these ceramic samples revealed that the presence of silicon enhanced the cell proliferation and the highest absorbance value of 0.10 was obtained from the sample 5SiHA. Thian et al. [26] demonstrated that the silicon-containing hydroxyapatite thin films promoted the growth of human osteoblast-like cells and increased the number of focal adhesion points and the early formation of extracellular matrix. It was suggested that was due to the enhanced dissolution of silicon containing HA. Porter et al. [4] proposed that the incorporation of silicate ions into HA led to an increased rate of dissolution of silicon substituted HA by the formation of the increased number of defect structures compared to phase pure HA. The Ca, P and Si ions subsequently diffuse through the ceramic grains to the bone-HA interface, driven by a concentration gradient. They confirmed that defects, in particular those involving grain boundaries, were the starting point of dissolution *in vivo*. *In vitro* studies by Gibson et al. [27] also showed that the substitution of silicate for phosphate ions into HA enhances osteoblast cell activity, compared to phase pure HA. In the present study, both the soluble Si and the presence of the fast resorbing phase TCP [28] present in the compacts were dissolved in the culture medium and thus, were readily available to the osteoblast cells at early time points of culture which might have stimulatory effect on the bone mineralization process.

4. Conclusions

A novel nano-structured silicon doped hydroxyapatite prepared with various amounts of amorphous silica (1, 3, and 5 wt%) was consolidated at 1000 ℃ for 3 min using a spark plasma sintering technique. The XRD results, Raman spectra and XPS analysis indicated the substitution possibility of silicate in the apatite structure during the spark plasma processing. The presence of silica led to the decomposition of HA into a secondary calcium phosphate phase (β-TCP) and enhanced mechanical properties during spark plasma sintering processing. Enhance dissolution due to silicon substitution and TCP phase content may contribute to the higher cell proliferation ability when compared with phase pure HA, confirming a good level of biocompatibility.

Acknowledgements

This work was supported by the NTU-NSI joint project between Nanyang Technological University and Nanoscience Innovation. The authors are grateful to Mr. Lu Yiwei of school of chemical and biological engineering for his assistance in the cell culture work.

References

[1] I.R. Gibson, S.M. Best, W. Bonfield, J. Am. Cer. Soc. 85 (2002) 2771 – 2777.

[2] S.R. Kim, J.H. Lee, Y.T. Kim, D.H. Riu, S.J. Jung, Y.J. Lee, S.C.Chung, Y.H. Kim, Biomater. 24 (2003) 1389 – 1398.

[3] N. Patel, S.M. Best, W. Bonfield, J. Mater. Sci. Mater. Med. 13 (2002)1199 – 1206.

[4] A.E. Porter, N. Patel, J.N. Skepper, S.M. Best, W. Bonfield, Biomater. 24 (2003) 4609 – 4620.

[5] L. Borum, O.C. Wilson Jr., Biomater. 24 (2003) 3681 – 3688.

[6] M. Vallet-Regi, D. Arcos, J. Mater. Chem. 15 (2005) 1509 – 1516.

[7] I.R. Gibson, S.M. Best, W. Bonfield, J. Biomed. Mater. Res. 44 (1999) 422 – 428.

[8] L. Boyer, J. Carpena, J.L. Lacout, Solid. Stat. Ion. 95 (1997) 121 – 129.

[9] M. Omori, Mater. Sci. Eng. A. 287 (2000) 183 – 188.

[10] M. Nygren, Z. Shen, Solid. Stat. Sci. 5 (2003) 125 – 131.

[11] A. Lebugle, A. Rovira, M. Rabaud, C. Rey, J. Mater. Sci. Mater. Med. 7 (1996) 223 – 226.

[12] A.J. Ruys, J. Aus. Cer. Soc. 29 (1993) 71 – 80.

[13] C. Hammond, The Basics of Crystallography and Diffraction, Oxford University Press, New York, 2002.

[14] K.C. Blakesee, R.A. Condrate Sr., J. Am. Ceram. Soc. 54 (1971) 559 – 563.

[15] R. Cusco, F. Guitian, S. de Aza, L. Artus, J. Eur. Ceram. Soc. 18(1998) 1301 – 1305.

[16] G. Penel, G. Leroy, C. Rey, E. Bres, Calcif. Tissue. Int. 63 (1998) 475 – 481.

[17] B.D. Assollant, A. Ababou, E. Champion, M. Heughebaert, J. Eur. Cer. Soc. 23 (2003) 229 – 241.

[18] M. Sayer, A.D. Stratilatov, J. Reid, L. Calderin, M.J. Stott, X. Yin, M. MacKenzie, T.J.N. Smith, J.A. Hendry, S.D. Langstaff, Biomater. 24 (2003) 369 – 382.

[19] E. Balas, J. Perez-Pariente, M. Vallet_Regi, J. Biomed. Mater. Res. A 66 (2003)

364 – 375.

[20] A. Mekki, D. Holland D, K.H. Ziq, C.F. McConville, J. Non-Cryst. Solid 220 (1997) 267 – 279.

[21] G. Beshkov, V. Krastev, K. Grigorov, H. Maciel, T.A. Tang, V. Huang, Surf. Coat. Tech. 161 (2002) 11 – 19.

[22] T. Kanazawa, T. Umegaki, K. Yamashita, H. Monma, T. Hiramatsu, J. Mater. Sci. 26 (1991) 417 – 422.

[23] C.K. Wang, C.P. Ju, J.H. Chern Lin, Mater. Chem. Phys. 53 (1998) 138 – 149.

[24] K.A. Gross, L.M. Rodriguez-Lorenzo, Biomater. 25 (2004) 1385 – 1394.

[25] G. Muralithran, S. Ramesh, Comput. Inter. 26 (2000) 221 – 230.

[26] E.S. Thian, J. Huang, S.M. Best, Z.H. Barber, W. Bonfield, Biomater. 26 (2005) 2947 – 2956.

[27] I.R. Gibson, K.A. Hing, S.M. Best, W. Bonfield, in: H. Ohgushi, G.W. Hastings, T. Yoshikawa (Eds.), 12th International Symposium on Ceramics in Medicine, Nara, Japan, 1999, pp. 191 – 194.

[28] S.A. Redey, M. Nardin, D.B. Assolant, C. Rey, P. Delannoy, L. Sedel, P.J. Marie, J. Biomed. Mater. Res. 50 (2000) 353 – 364.

List of table

List of figure

Table 1
Lattice parameters of spark plasma sintered compacts

Samples	*a*-axis (Å)	*c*-axis (Å)	Unit cell volume (Å^3)
SD	9.4182	6.8810	528.5889
1SiHA	9.4235	6.8900	529.8761
3SiHA	9.4227	6.8970	530.3244
5SiHA	9.4352	6.8984	531.8403

Table 2
Peak positions (in cm^{-1}) and type of the generating vibration modes of the various spark plasma sintered compacts

Samples				Type of vibrations
HA	1SiHA	3SiHA	5SiHA	
3571	3571	3571	–	O–H stretching in apatite
1090	1090	1090	1074	P–O stretching in apatite (v_3)
1077	1078	1075	1046	
1048	1049	1047		
962	961	961	962	Symmetrical PO_4 stretching in apatite (v_1)
603	607	605	603	O–P–O and P–O in apatite (v_4)
578	577	576	589	
450	450	449	450	O–P–O in apatite (v_2)
430	429	428	428	

Table 3
Binding energies (eV) obtained from XPS of spark plasma sintered compacts referred P 2p to 133.6 eV

Samples	Ca 2p	O 1s	C 1s	Si 2p
SD HA	347.5	531.3	285.1	
	351.0	532.8	286.6	
1SiHA	347.4	531.1	285.0	102.3
	350.9	532.7	286.9	
		529.8		
3SiHA	347.5	532.1	284.5	102.3
	351.1	534.0	285.6	103.5
		535.2	288.8	
5SiHA	347.2	531.2	282.3	101.4
	350.8	532.7	285.2	102.8
			286.6	

Table 4
Densities and relative densities of spark plasma sintered compacts

Samples	Densities (g/m^3)	Relative densities (%)
HA	3.09	97.9
1SiHA	3.05	96.6
3SiHA	3.01	95.4
5SiHA	2.99	94.8

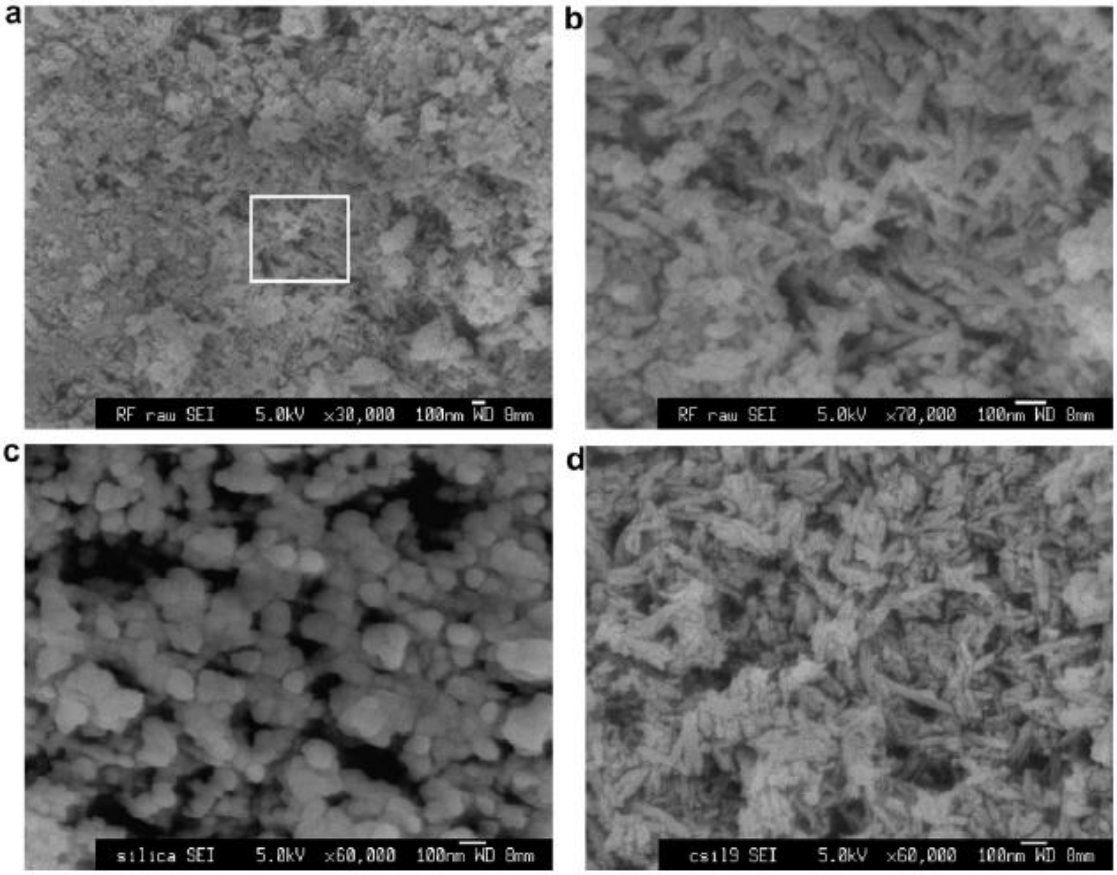
a
RF raw SEI 5.0kV x30,000 100nm WD 8mm
b
RF raw SEI 5.0kV x70,000 100nm WD 8mm
c
silica SEI 5.0kV x60,000 100nm WD 8mm
d
csil9 SEI 5.0kV x60,000 100nm WD 8mm

Fig. 1

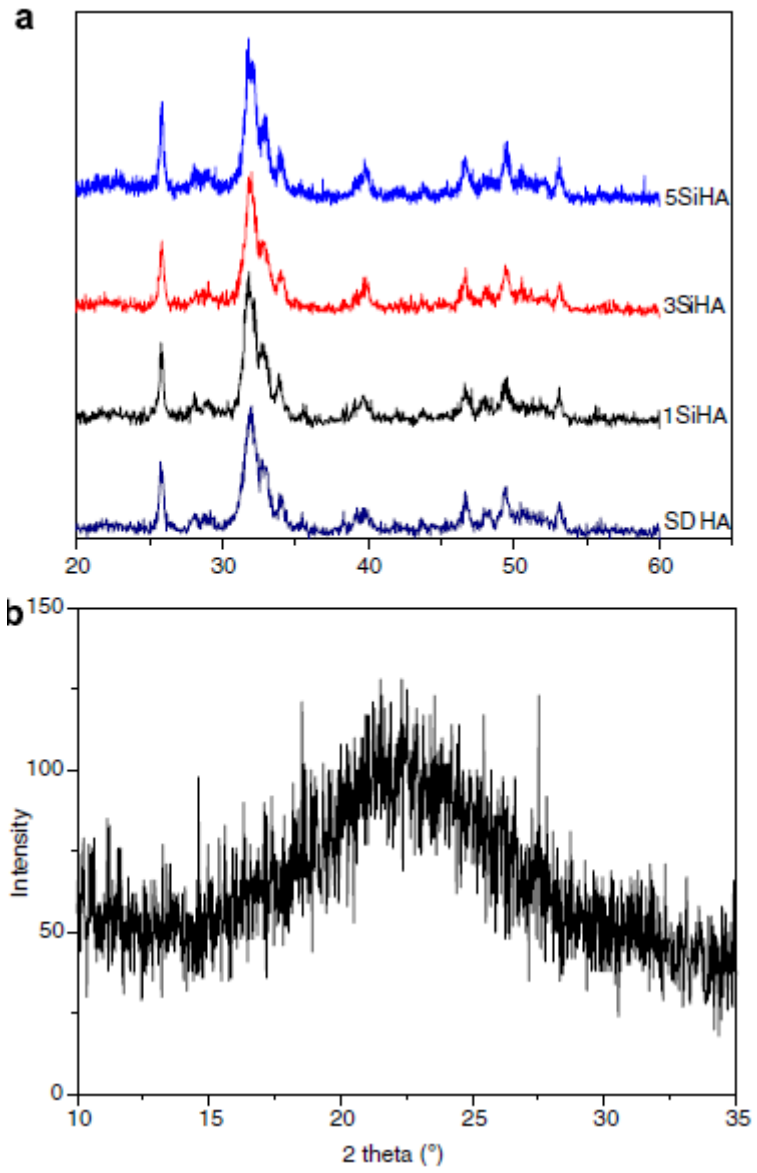
a
5SiHA
3SiHA
1SiHA
SD HA
20
30
40
50
60
b
150
100
50
0
Intensity
10
15
20
25
30
35
2 theta (°)

Fig. 2

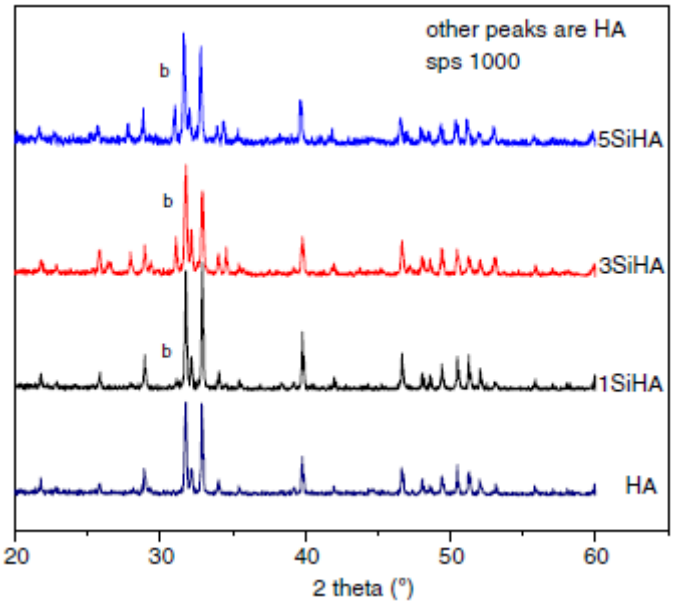
other peaks are HA
sps 1000
b
b
b
5SiHA
3SiHA
1SiHA
HA
20
30
40
50
60
2 theta (°)

Fig. 3

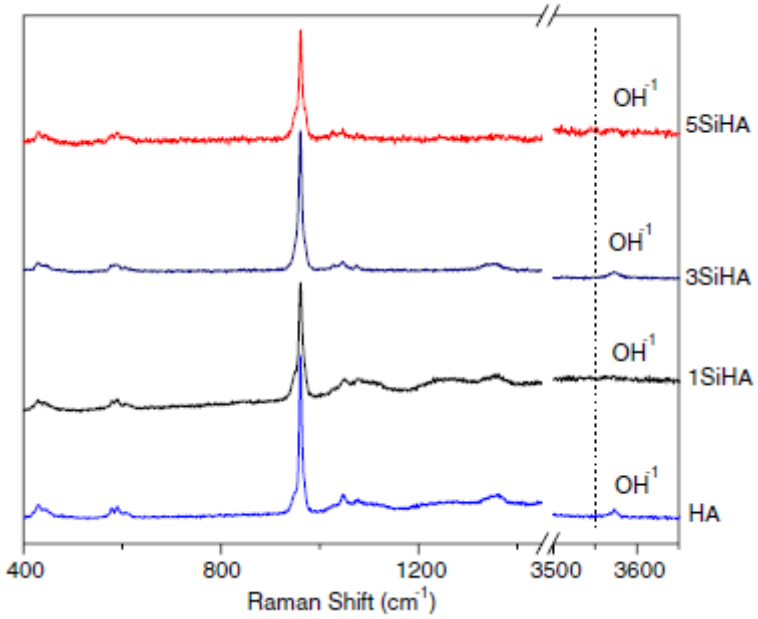
OH-1
5SiHA
OH-1
3SiHA
OH-1
1SiHA
OH-1
HA
400
800
1200
3500
3600
Raman Shift (cm-1)

Fig. 4

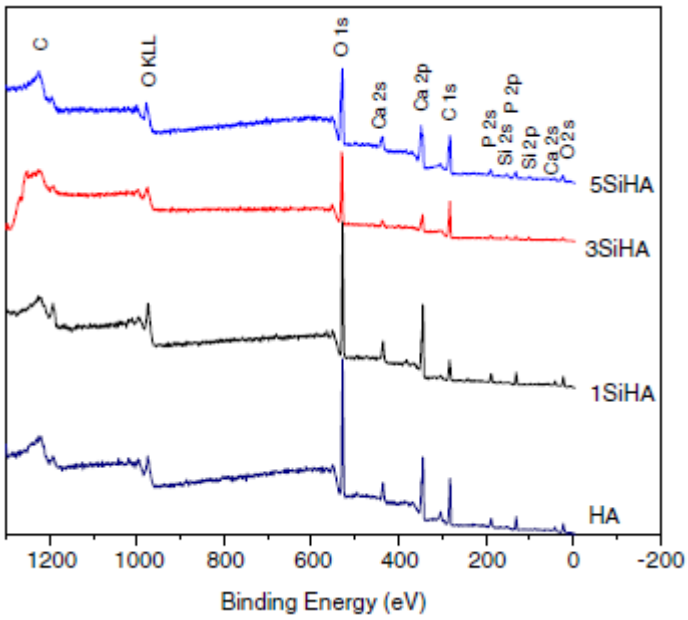
C
O KLL
O 1s
Ca 2s
Ca 2p
C 1s
P 2s
Si 2s
P 2p
Si 2p
Ca 2s
O2s
5SiHA
3SiHA
1SiHA
HA
1200
1000
800
600
400
200
0
-200
Binding Energy (eV)

Fig. 5

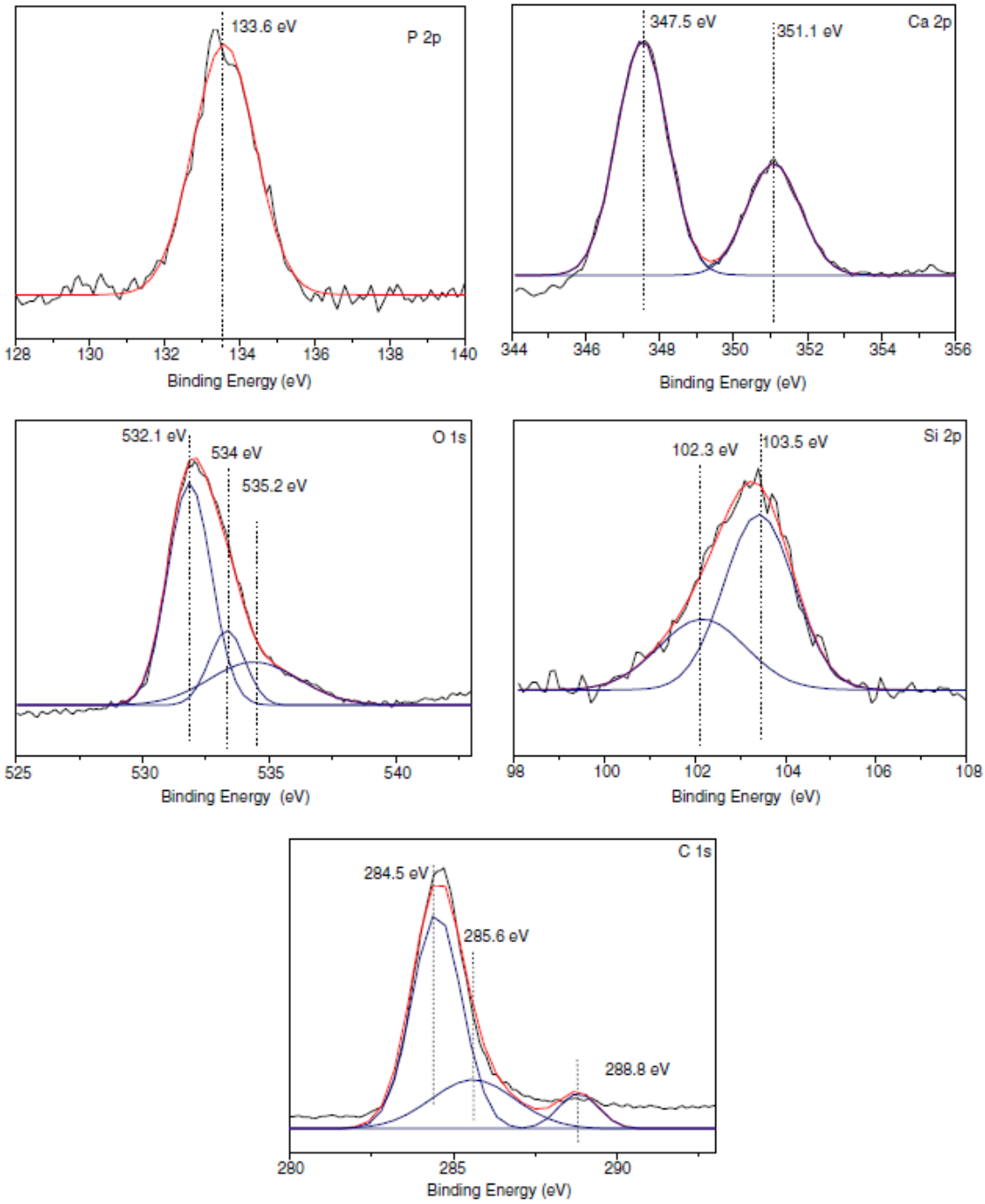
133.6 eV
P 2p
128
130
132
134
136
138
140
Binding Energy (eV)
347.5 eV
351.1 eV
Ca 2p
344
346
348
350
352
354
356
Binding Energy (eV)
532.1 eV
534 eV
535.2 eV
O 1s
525
530
535
540
Binding Energy (eV)
102.3 eV
103.5 eV
Si 2p
98
100
102
104
106
108
Binding Energy (eV)
284.5 eV
285.6 eV
288.8 eV
C 1s
280
285
290
Binding Energy (eV)

Fig. 6

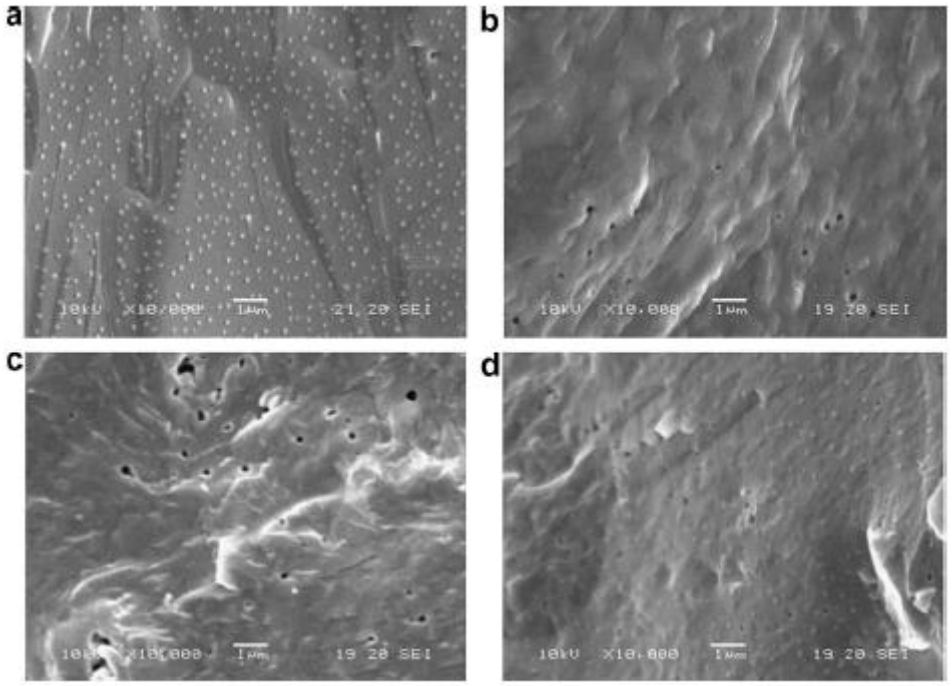

Fig. 7

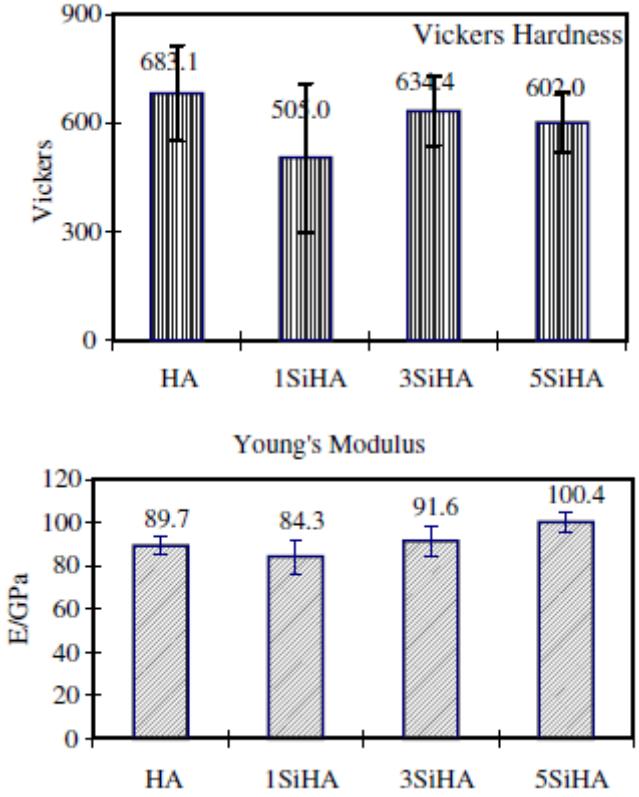
Vickers Hardness
Vickers
900
600
300
0
683.1
505.0
634.4
602.0
HA
1SiHA
3SiHA
5SiHA
Young's Modulus
E/GPa
120
100
80
60
40
20
0
89.7
84.3
91.6
100.4
HA
1SiHA
3SiHA
5SiHA

Fig. 8

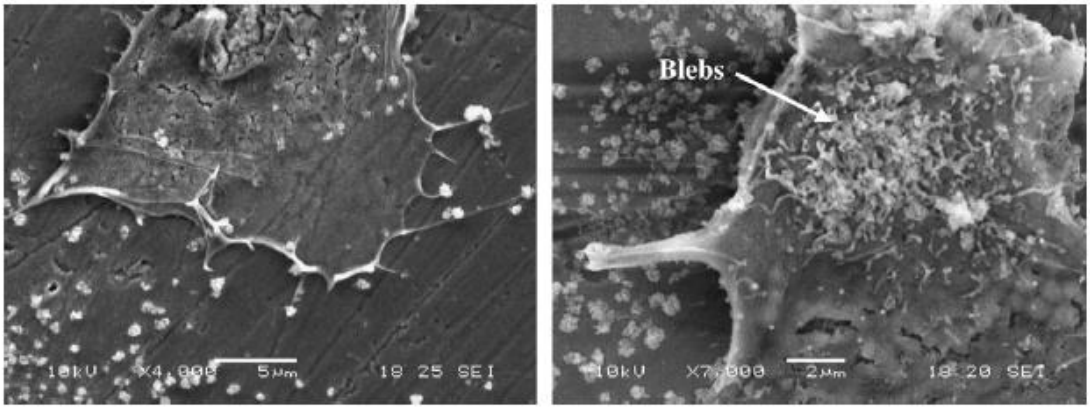

Fig. 9

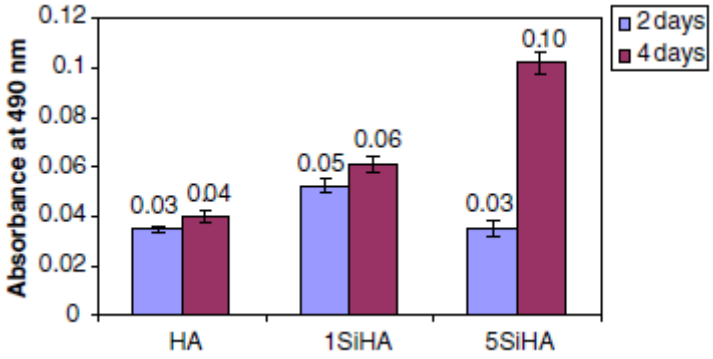
Absorbance at 490 nm
0.12
0.1
0.08
0.06
0.04
0.02
0
0.03
0.04
0.05
0.06
0.03
0.10
HA
1SiHA
5SiHA
2 days
4 days

Fig. 10